

*Appendix A*

## VA-TIRFM supporting information

The following are included in this appendix:

A.1 Relationships between excitation laser beam position and angle of incidence in the coverslip

A.2 Evanescent field intensity as a function of angle of incidence

A.3 Imaging sequence table including which images are averaged

A.4 Andor iXonem+ 897 camera background

A.5 Photographs of Teflon cell culture chamber

A.6 Photographs of TIRF microscope and excitation positioning assembly

### A.1 Relationships between excitation laser beam position and angle of incidence in the coverslip

Prism based TIRF angle measurement (July 1-6, 2010)

These values were used for all of the data analysis presented in this thesis.

Excitation laser distance from start of TIRF (microns)	Excitation laser distance from actuator 'Home' (mm)	Incidence angle at N-LAF21 coverslip-air interface
30	9.54	62.20011804
40	9.55	61.56618627
50	9.56	60.97517815
60	9.57	60.36034276
70	9.58	59.75822335
80	9.59	59.15776225
90	9.6	58.57997814
100	9.61	58.09803605
110	9.62	57.47241837
120	9.63	56.94762434
130	9.64	56.49142547
140	9.65	55.87686581
150	9.66	55.38603725
160	9.67	54.84467262
170	9.68	54.37578342
180	9.69	53.84137628
190	9.7	53.36306498
200	9.71	52.85593721
210	9.72	52.38820027
220	9.73	51.89360491
230	9.74	51.3740835
240	9.75	50.89504964
250	9.76	50.42415964
260	9.77	49.87027422
270	9.78	49.43323141
280	9.79	48.96066402
290	9.8	48.51270569
300	9.81	48.06056125
310	9.82	47.57803314
320	9.83	47.121313
330	9.84	46.65059582
340	9.85	46.23064973

Table A.1 Angle as a function of beam position. This measurement was made in the TIRF region using a SF-2 equilateral prism ( $n=1.648$ ) to project the beam onto lab wall. Then the beam angle in air was calculated, then the beam angle in the prism and then that in the coverslip using a coverslip index of refraction-1.7993 and a 488 nm laser.

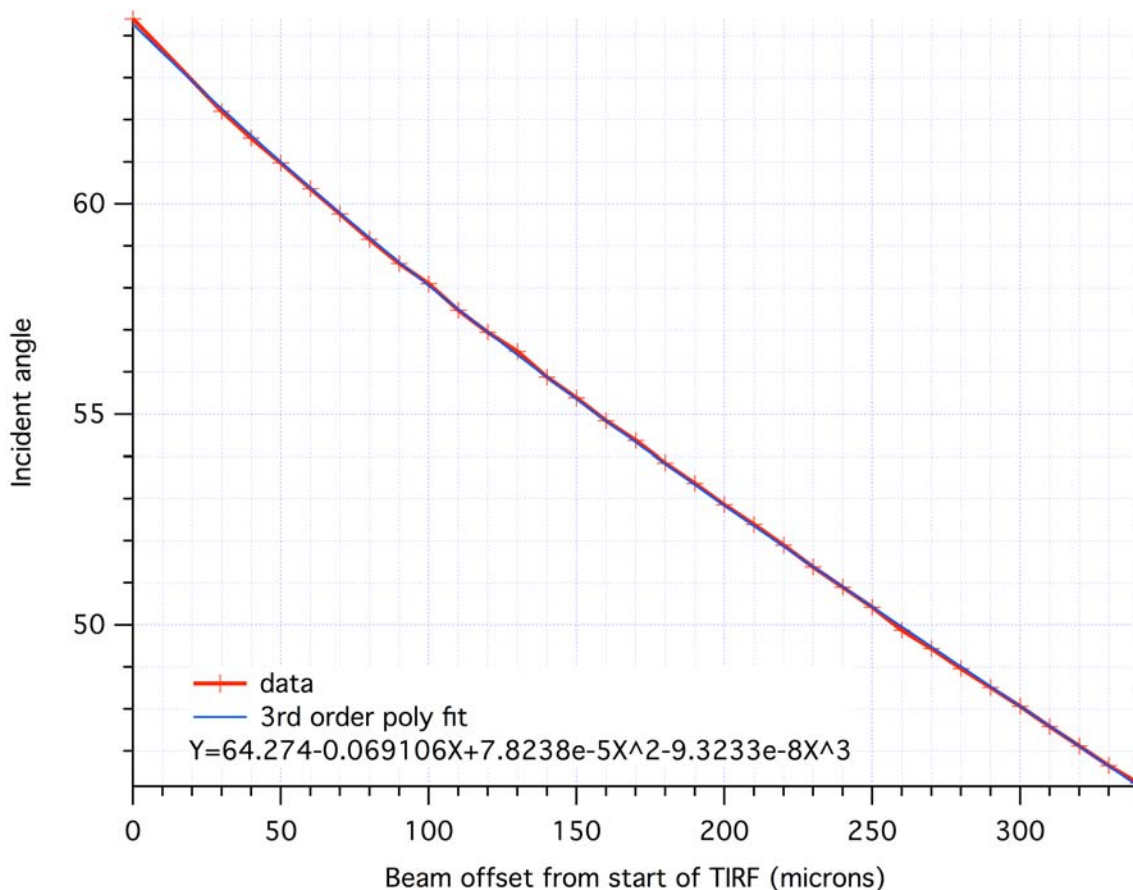


Figure A.1 Angle of incidence as a function of beam offset. This is from the prism-based measurement of beam angle as a function of position. The curve fit relation was used to relate the position data in my lab notebook to the angle of incidence. That angle of incidence was in turn used to establish penetration depth. Therefore this figure was used to select which images to use for image processing in every case for the data presented in Chapter 2 of this thesis. This relation was used rather than absolute beam position because at times there was some drift in the measured position. In that case I would use the offset from onset of TIRF (defined by the maximum angle allowed by the back aperture) to determine what the angle and thereby the penetration depth were.

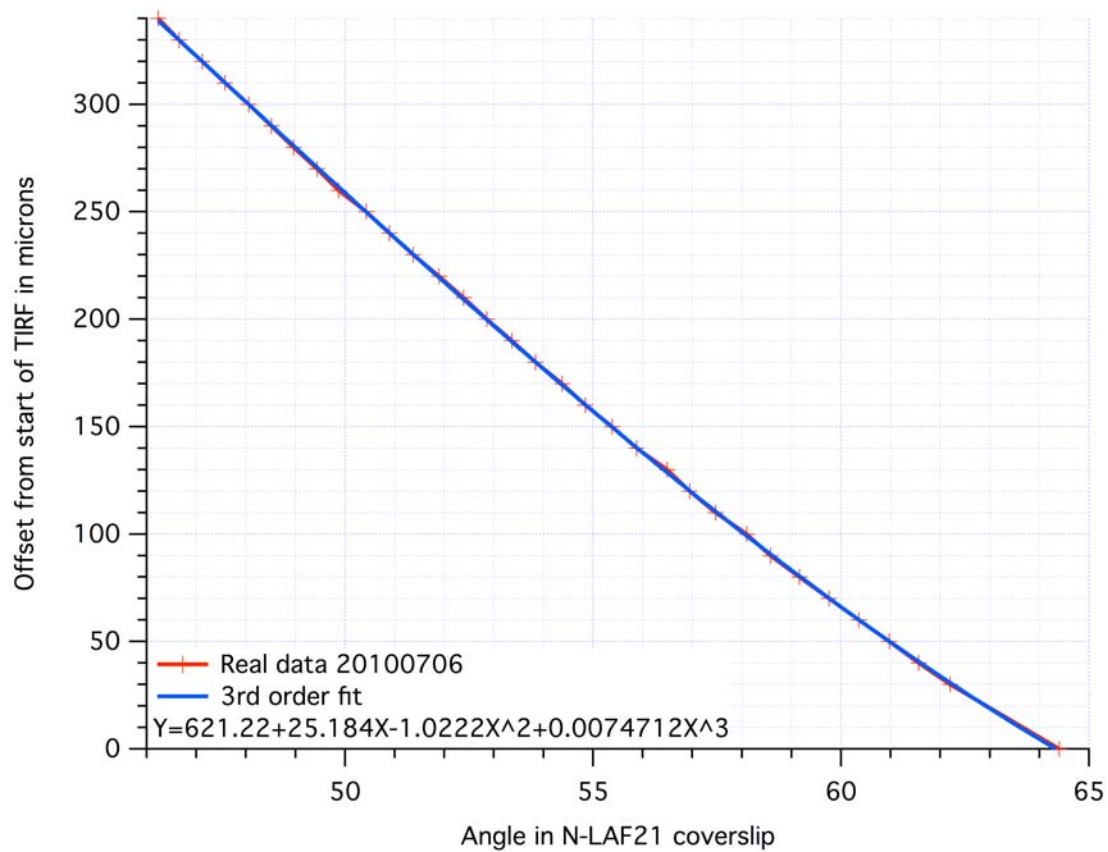


Figure A.2 Prism based TIRF measurement fit and data: Offset laser position as a function of angle. This is the inverse plot from that in Figure A.1.

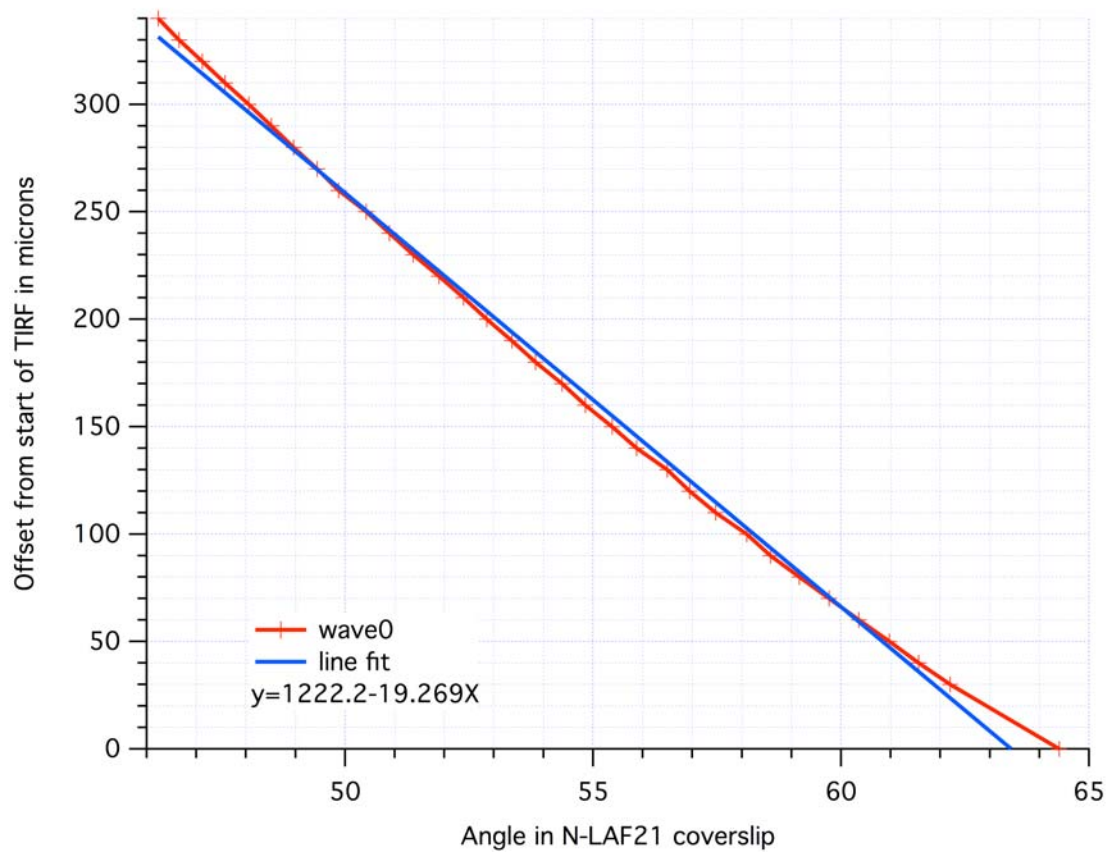


Figure A.3 Prism TIRF data compared to a linear fit: it is really close.

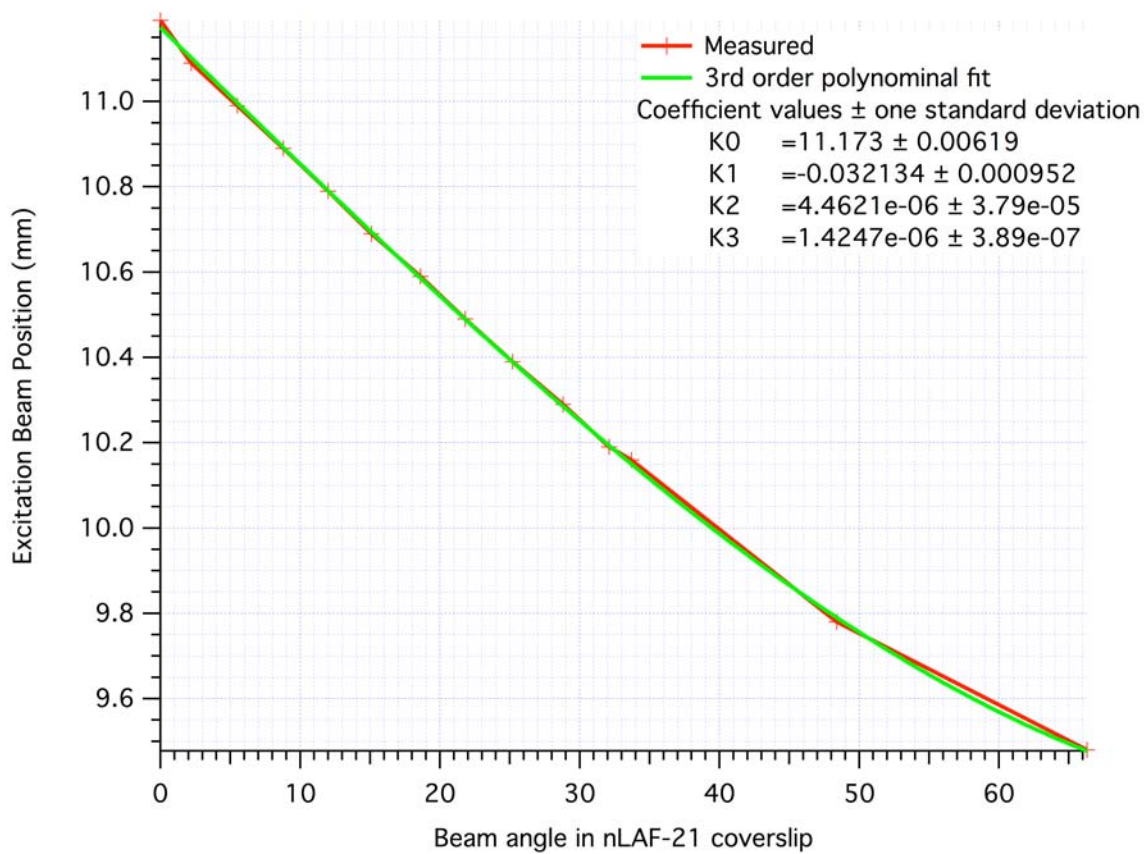


Figure A.4 Full scale fit from the laser in Epi (pointed vertically) to sealing down to the critical angle (data points from  $0^\circ$  to  $\sim 34^\circ$ ). It also includes a waterbased TIRF onset datapoint and another at the extreme edge of the back aperture point. The units on the excitation beam position are distance in (mm) from the actuator 'homed' position.

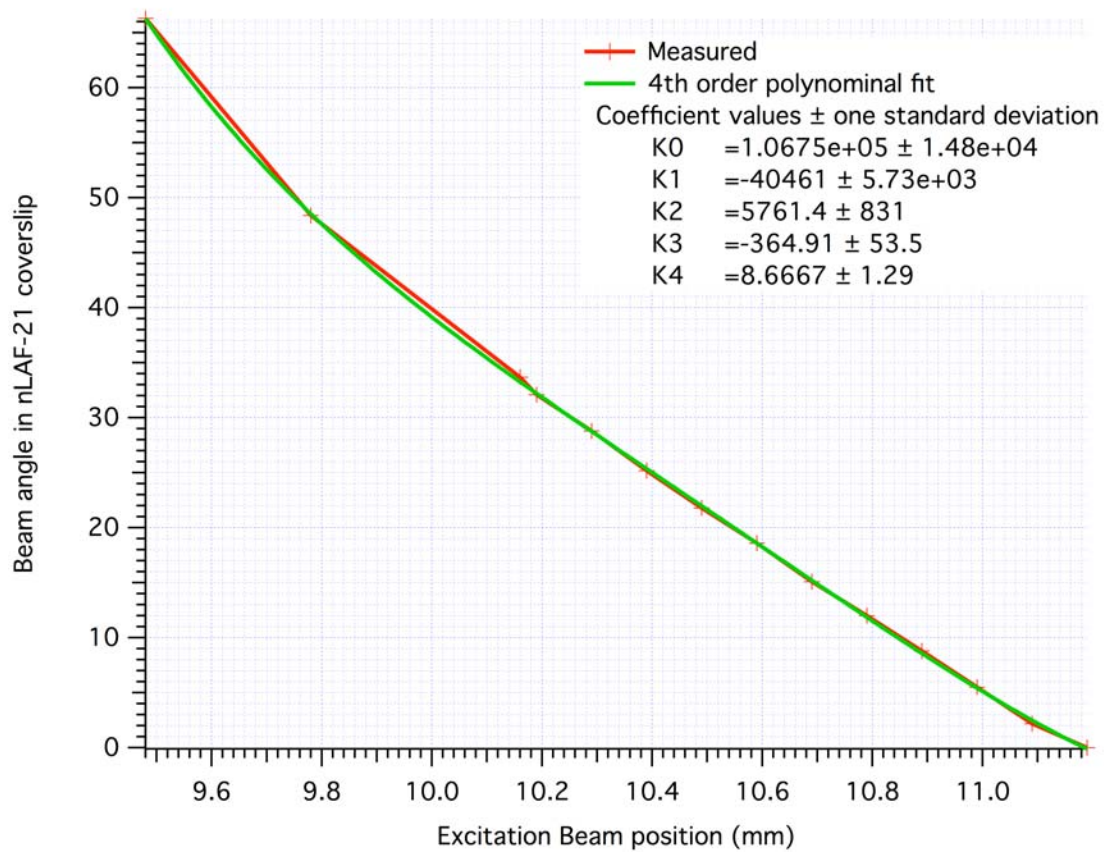


Figure A.5 Beam angle as a function of excitation beam position. Full scale fit from the laser in Epi pointed vertically to sealing down to the critical angle (data points from  $0^\circ$  to  $\sim 34^\circ$ ). It also includes a water-based TIRF onset datapoint and the extreme edge of the back aperture point. The units on the excitation beam position are distance in (mm) from the actuator 'homed' position. This is the inverse of Figure A.4.

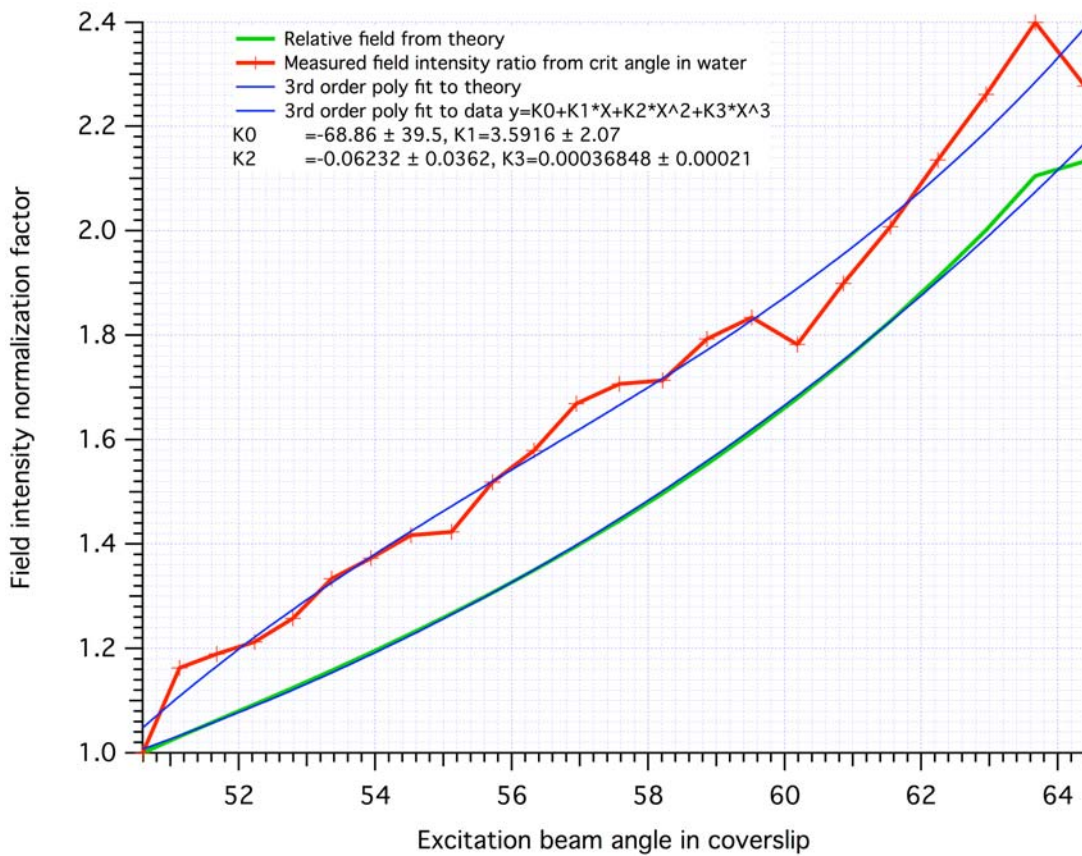


Figure A.6 The measured field intensity averaged was about 10% (on average) lower than that predicted by theory over the TIRF range of incident angle. At present we can only speculate as to the origin of this discrepancy. One possibility is that the evanescent field intensity is diminished across the coverslip in the direction of propagation due to scattering caused by the sample and coverslip surface roughness. An alternative explanation is that the difference is due to my measurement and/or data analysis error. A third is that a small fraction of the excitation energy within the evanescent region might contain some vertically polarized energy

As a result the normalization factor was increased by 10% from theory to account for this difference.

## A.2 Evanescent field intensity as a function of angle of incidence

Microns offset	position (mm)	angle	Penetration Depth (nm)	Calc Intensity	Normalization	ADJ+ 10%
0	9.51	64.274	46.11099207	1.849497093	2.153675043	2.369
10	9.52	63.590	47.13495262	1.941917327	2.051176781	2.256
20	9.53	62.922	48.22529751	2.033929283	1.958384574	2.154
30	9.54	62.268	49.38857035	2.125454198	1.874053902	2.061
40	9.55	61.628	50.63245181	2.21642634	1.797134269	1.976
50	9.56	61.002	51.96600732	2.306792179	1.726733673	1.899
60	9.57	60.389	53.40000522	2.39650959	1.662090462	1.828
70	9.58	59.787	54.94733027	2.485547091	1.602550902	1.762
80	9.59	59.198	56.6235278	2.573883125	1.547551127	1.702
90	9.6	58.620	58.44753042	2.661505365	1.496602556	1.646
100	9.61	58.052	60.44264372	2.748410064	1.449279998	1.594
110	9.62	57.494	62.63790777	2.834601432	1.405211924	1.545
120	9.63	56.946	65.07001602	2.920091055	1.364072441	1.500
130	9.64	56.407	67.78608288	3.004897335	1.32557465	1.458
140	9.65	55.876	70.84774223	3.089044974	1.289465115	1.418
150	9.66	55.353	74.33740586	3.172564475	1.255519238	1.381
160	9.67	54.838	78.36817005	3.255491682	1.22353737	1.345
170	9.68	54.329	83.1001824	3.337867337	1.193341535	1.312
180	9.69	53.826	88.76912127	3.419736672	1.164772646	1.281
190	9.7	53.328	95.73903929	3.501149013	1.137688147	1.251
200	9.71	52.836	104.6087792	3.582157416	1.111959992	1.223
210	9.72	52.348	116.4508049	3.662818315	1.087472921	1.196
220	9.73	51.864	133.4349282	3.743191193	1.064122971	1.170
225	9.735	51.623	145.2559639	3.783288968	1.052844698	1.158
230	9.74	51.384	160.8804372	3.823338265	1.041816197	1.145
235	9.745	51.144	182.9217212	3.86334724	1.031027108	1.134
240	9.75	50.906	217.4781111	3.903324181	1.020467568	1.122
245	9.755	50.668	283.9205354	3.943277501	1.010128182	1.111
250	9.76	50.430	521.9432409	3.983215732	1	1

Table A.2 Evanescent field intensity at the coverslip surface as a function of angle of incidence. The +10% values in the far right column were used for all images processed in Chapter 2 of this thesis.

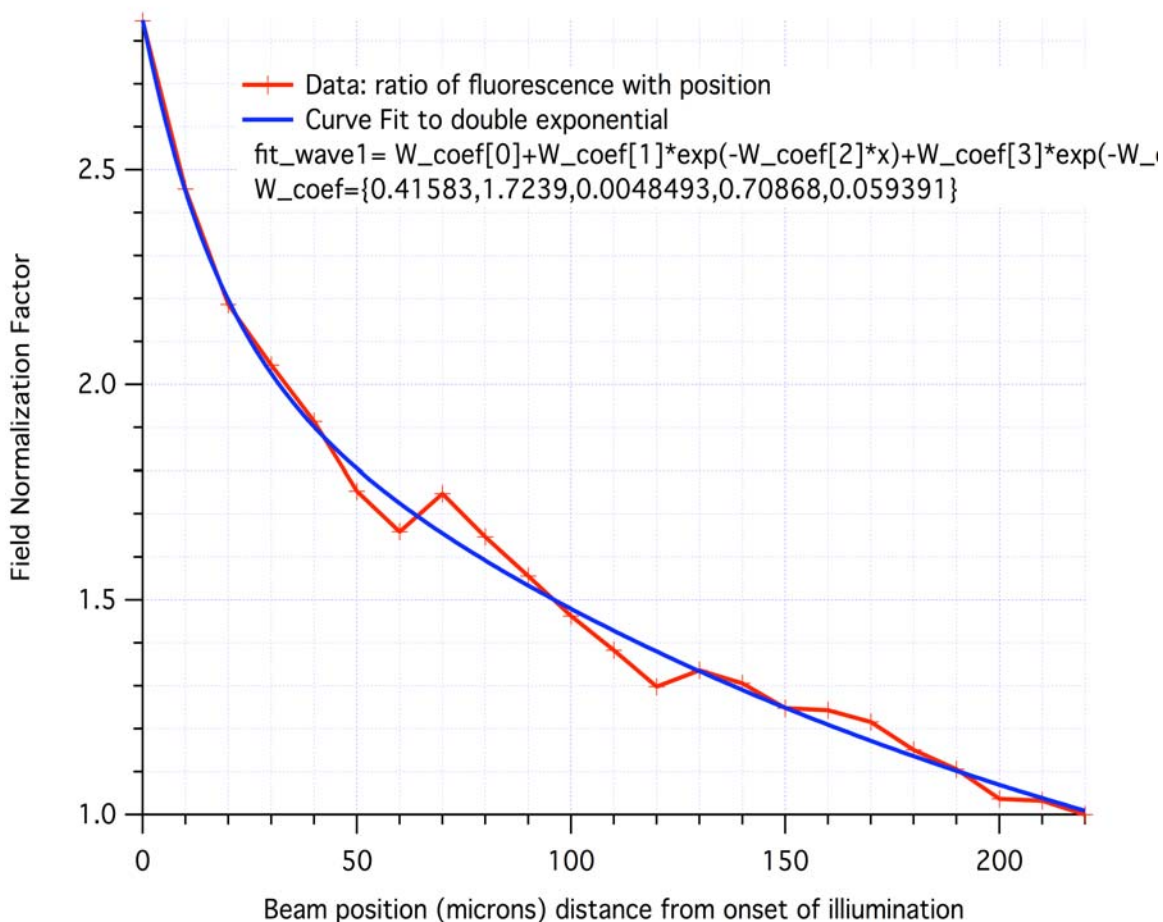


Figure A.7 The measured field normalization factor as a function of offset beam position from the onset of illumination (at the outside edge of objective). The actual onset was considered to be once the full beam was past the edge of the objective. That onset was found to be 20 microns past the point where light would first start to leak past the edge. The evanescent field intensity was determined by measuring the fluorescence intensity from 20 nm beads stuck on a N-LAF21 coverslip with more beads in solution above the coverslip. To make this measurement, the average of a very small region of interest was defined in ImageJ. Four sets of measurements were made across the 220 micron TIRF range. A new region of interest was selected for each of those runs. The average intensity within that ROI was measured in 10 micron increments. The intensity for the four runs at each position was then averaged. That yielded the data plotted here. When beads became continuously visible in any part of the image, the limit of TIRF was considered to have been reached. From this point it was ~20 microns further in beam position before the full field would be far-field illuminated...presumably due to beam width again.

### A.3 Imaging sequence table including which images are averaged

Assume that images were taken every 10 microns from the onset of TIRF (as defined above), then those images can be numbered. Image 1 was the very first image taken at the onset of TIRF. Image 26 was then taken after shifting the beam position 250 microns towards being centered.

These assume five slice image stacks as defined in Tables 2.2 and 2.3.

z-stack from most extreme TIRF towards critical angle	5 image logarithmic defined in Table 2.3	5 image even-spaced defined in Table 2.2
Stack Image 1	Average images 1-5	Average images 1-5
Stack Image 2	Average images 13-17	Average images 19-21
Stack Image 3	Average images 21-22	Average images 23-24
Stack Image 4	Image 24	Image 25
Stack Image 5	Average images 25-26	Image 26 if very clean else just use 4 stack

Table A.3 Images selected and averaged for z-stack to be used for 3D image generation.

#### **A.4 Andor iXonem+ 897 camera background**

A 200 image sequence was acquired with the camera stable at  $-85^{\circ}\text{C}$ . During these images the 488 laser was on but the shutter was off. Also the room light was off but computer monitors were on. A z-stack was then assembled and averaged. The histogram of that image showed values at 109, 110 and 111 counts per pixel with 110 having more pixels than the other two combined.

The camera background value of 110 counts per pixel was therefore used for all calculations within this thesis.

### A.5 Photographs of Teflon cell culture chamber

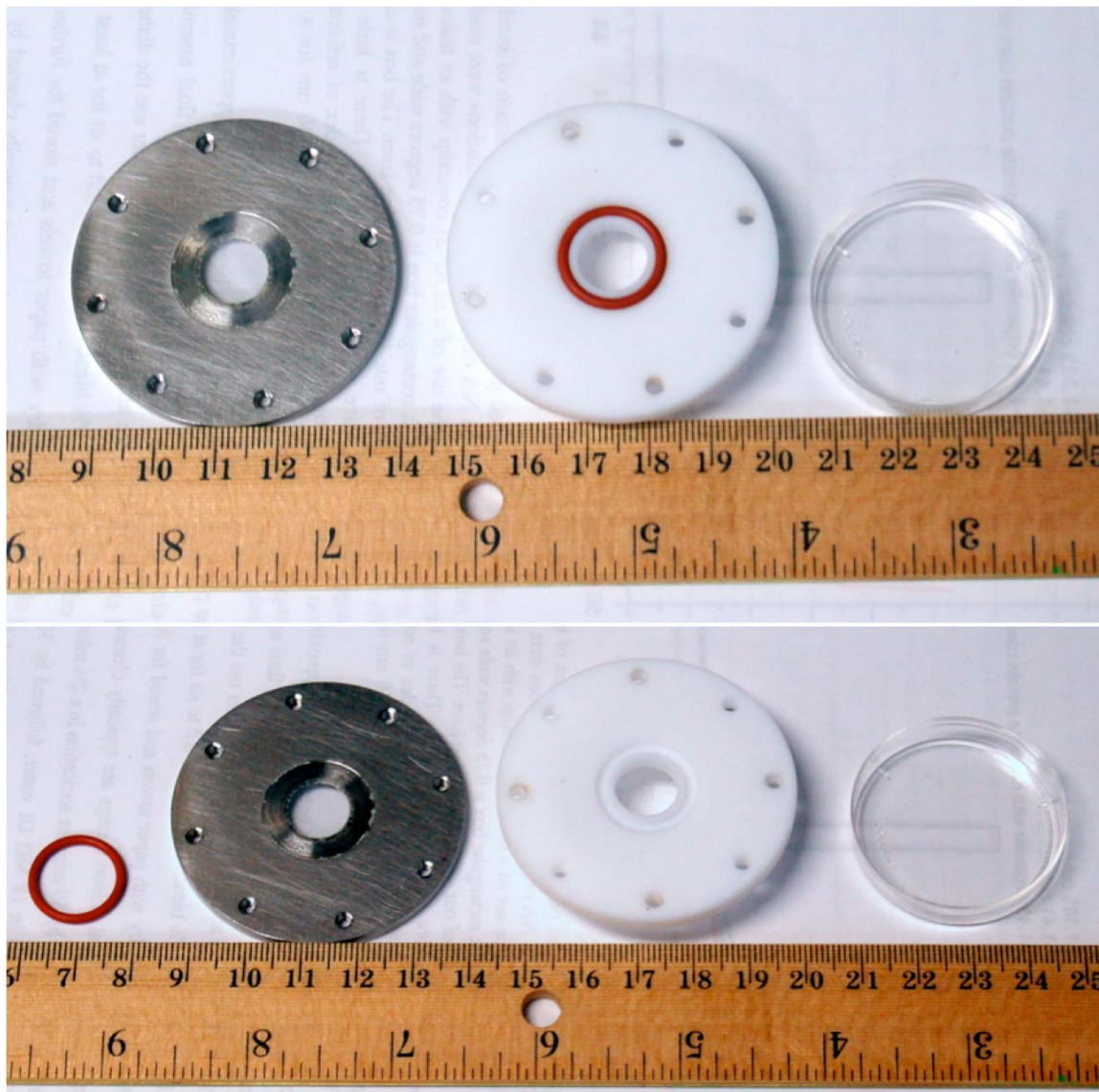


Figure A.8 Cell culture chamber parts. The baseplate was made of stainless steel. The chamber was made from virgin Teflon and sealed with a silicon o-ring. The chamber was covered with a commercial 35 mm culture dish top (to ensure proper circulation of air in the incubation chamber).

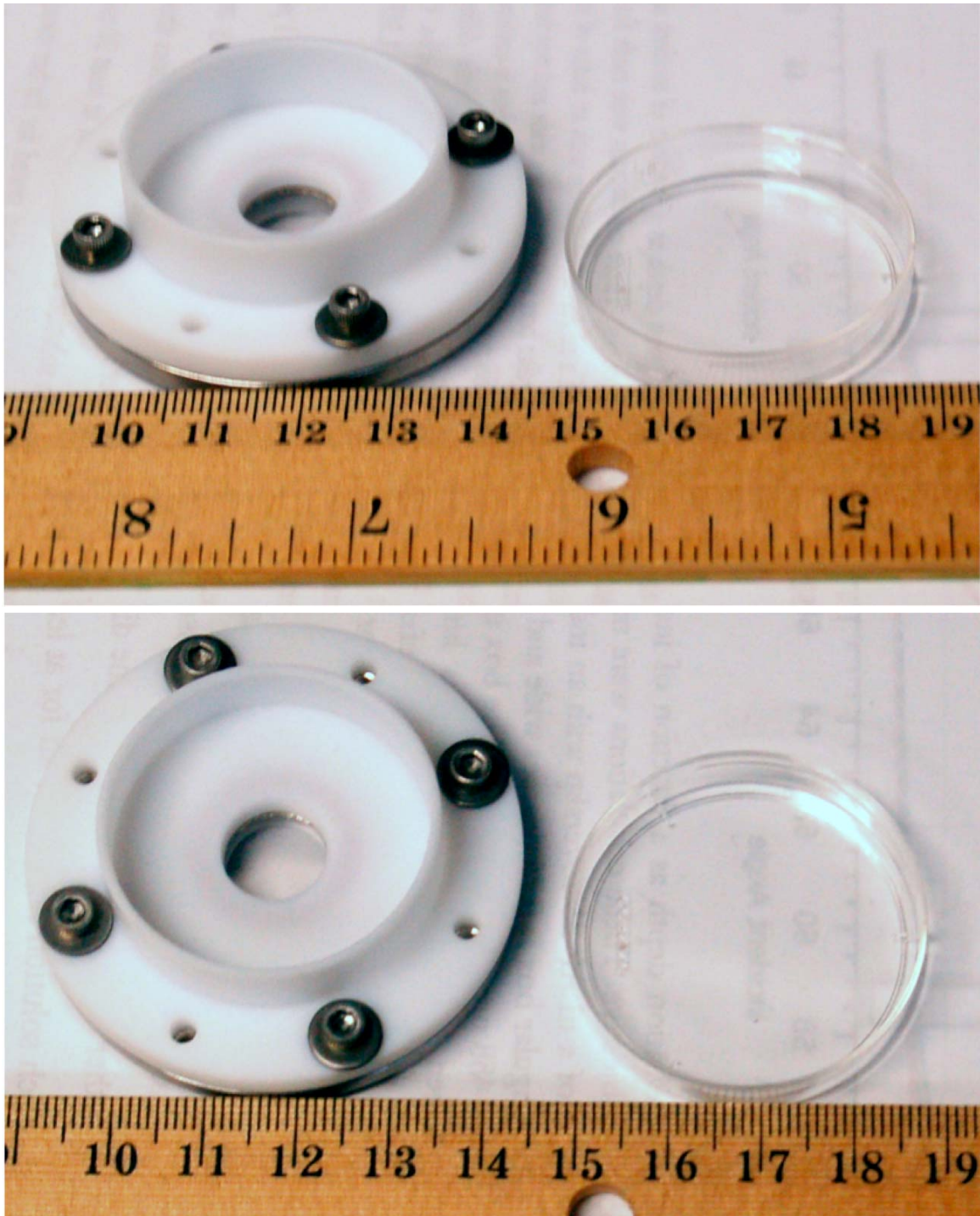


Figure A.9 An assembled cell culture dish is shown on the left with a commercial 35 mm cover.



Figure A.10 A fully assembled culture dish is shown above from the top and also from the bottom.

## A.6 Photographs of TIRF microscope and excitation positioning assembly



Figure A.11 The complete Olympus IX71 microscope used for the VA-TIRFM study reported in this thesis is shown here. Note the laser positioning assembly on the right.

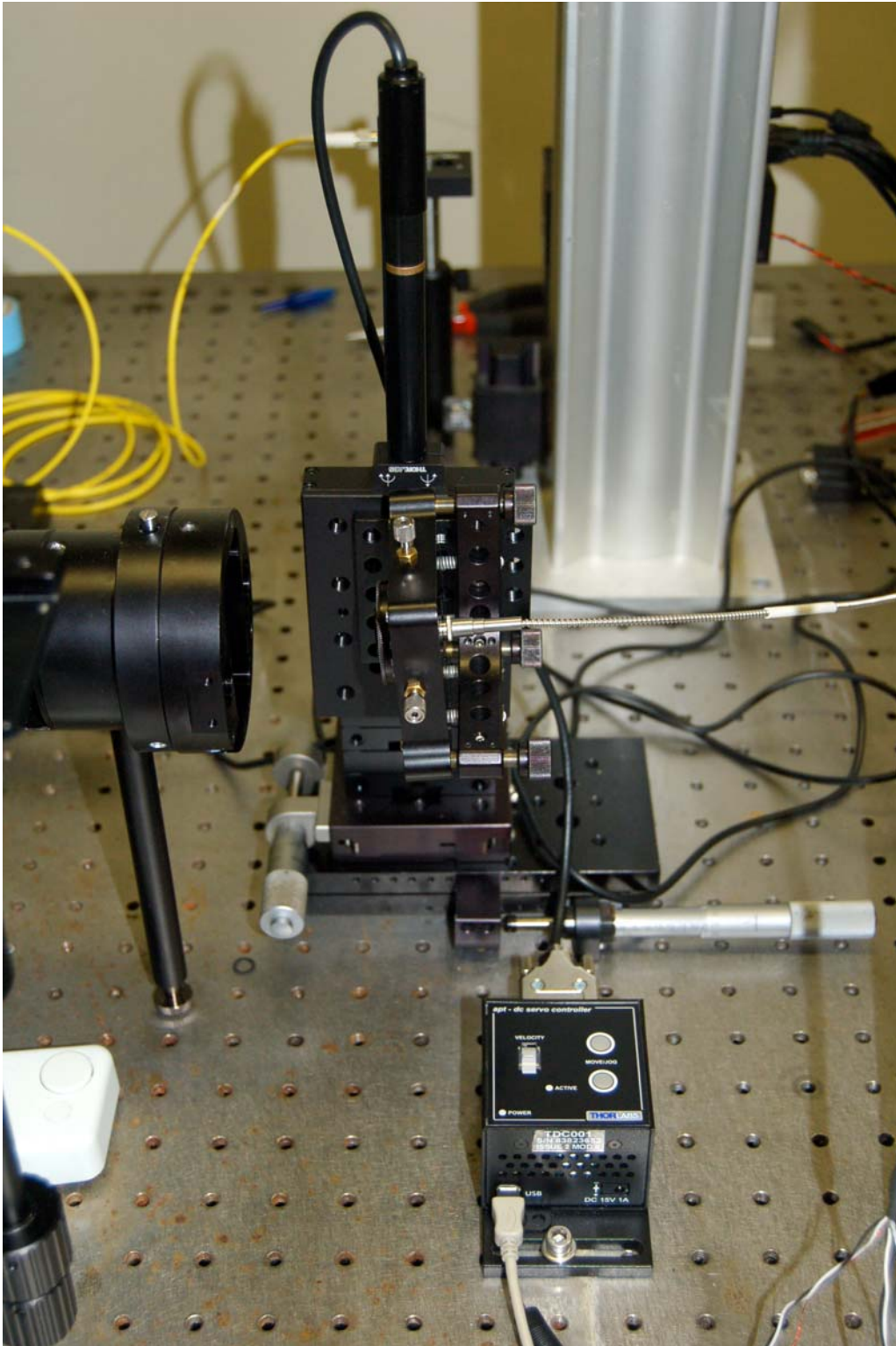
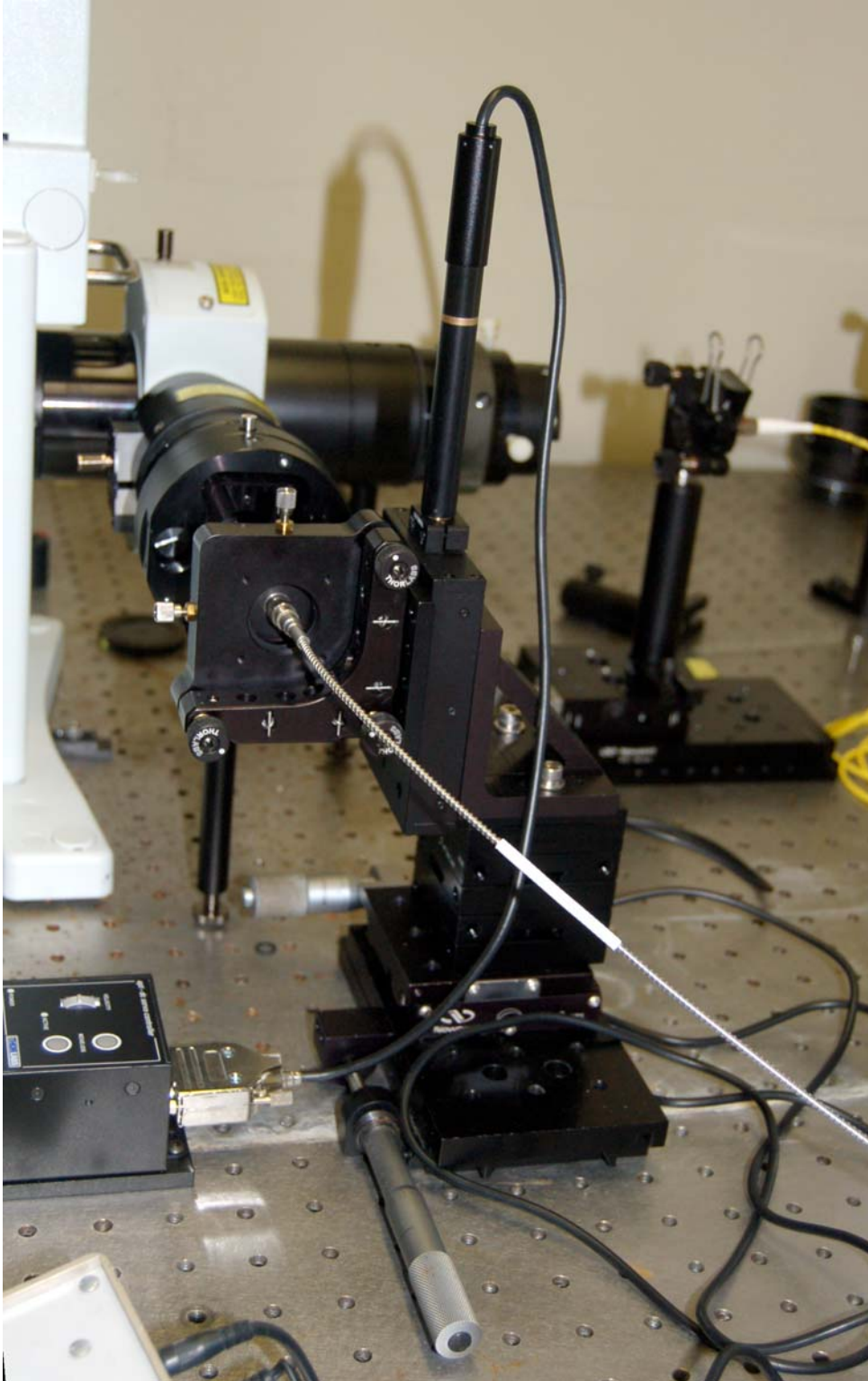


Figure A.12 Laser alignment and positioning assembly with control electronics.



A.13 View of laser positioning assembly facing the microscope.